Forward Modeling of Geophysical Electromagnetic Methods Using Comsol

S.L. Butler* and Z. Zhang*

*Dept. of Geological Sciences,
University of Saskatchewan,
Saskatoon, SK, Canada, S7N 5E2
sam.butler@usask.ca

Keywords: electromagnetic, geophysics, Comsol, model

Forward Modeling of Geophysical Electromagnetic Methods Using Comsol

S.L. Butler[1] and Z. Zhang[1]

[1] *Dept. of Geological Sciences, University of Saskatchewan, Saskatoon, SK, Canada, S7N 5E2*
sam.butler@usask.ca

Abstract

In geophysical electromagnetic methods, time-varying magnetic fields are measured at Earth's surface that are produced by electrical currents inside the Earth in order to constrain subsurface conductivity and geological structure. These methods are widely used for mineral exploration and environmental investigations, and are increasingly being used in hydrocarbon exploration as well. Forward modeling of exploration geophysics methods is useful for the purpose of survey planning, for understanding the method, especially for students, and as part of an iteration process in inverting measured data. Modeling electromagnetic methods remains an area of active research. In most geophysical methods, the electromagnetic frequency is sufficiently low that the wavelength of the radiation is much larger than the area of interest. As such, the quasi-static approximation is valid. Comsol Multiphysics' AC/DC module solves Maxwell's equations in the quasi-static approximation and in this contribution, we will show examples of its use in modeling magnetometric resistivity (MMR), very low frequency (VLF) techniques, as well as frequency and time-domain induction-based electromagnetic techniques. Solutions are compared with benchmarks from the literature.

1. Introduction

Geophysical electromagnetic techniques are used to remotely infer information concerning Earth's subsurface. In electromagnetic techniques, time-varying magnetic fields are measured at Earth's surface that are caused by electrical currents in Earth's subsurface (*Ward and Hohmann*, 1989; *West and MacNae*, 1991). Electromagnetic techniques are widely used in mining exploration (*Smith*, 2014) and environmental applications (*Reynolds*, 2011) and are increasingly being used in hydrocarbon exploration (*Strack*, 2014).

The results of forward models are useful for interpreting the results of electromagnetic surveying, for planning surveys, as part of a formal inversion, and for educational purposes. Three dimensional forward modeling of geophysical electromagnetic techniques remains an area of active research (see *Borner*; 2010, *Avdeev*, 2005 for reviews). Forward modeling of electromagnetic techniques involves the numerical solution of Maxwell's equations in conductive media, usually at sufficiently low frequencies that displacement currents can be neglected. Numerical techniques employed to carry out forward modeling include the finite difference technique (e.g., *Wang and Hohmann*, 1995), the integral equation technique (e.g., *Avdeev and Knizhnik*, 2009), the finite-volume technique (*Jahandari and Farquharson*, 2014), and the finite element method (e.g., *Ansari and Farquharson*, 2014). An advantage of the finite element method is that it can use unstructured grids that are well suited to modeling irregular geometrical shapes such as surface topography and subsurface resistivity anomalies.

Comsol Multiphysics (*Comsol Multiphysics User's Guide*, 2014) is a commercial finite element package that allows users to build complex models simply using a GUI. Further advantages of Comsol are its ability to couple different physical effects in the same model and that it has a large built-in library of meshing tools, numerical solvers and post processing tools. An additional module that is available for Comsol is the AC/DC module that contains functionality for solving Maxwell's equations in the quasi-static limit. While the main application of the AC/DC module is in electrical engineering, the quasi-static

approximation is also appropriate for modeling diffusive geophysical electromagnetic techniques.

In this contribution, we will give examples of models created using the AC/DC module of Comsol Multiphysics of the geophysical Very Low Frequency (VLF) technique, magnetometric resistivity (MMR), frequency domain electromagnetics and time-domain electromagnetics. In each case, we will compare the model results with published analytical solutions and numerical benchmarks.

2. Theory and Methodology

In all of the simulations presented here, the Magnetic Fields functionality in the the AC/DC module of Comsol was used. Comsol allows the user to choose between time-domain, frequency-domain and stationary studies. In the time domain, Ampère's law as solved by Comsol reads

$$\sigma \frac{\partial \mathbf{A}}{\partial t} + \nabla \times \mathbf{H} = \mathbf{J_e} \tag{1}$$

and

$$\mathbf{B} = \nabla \times \mathbf{A}. \tag{2}$$

The magnetic field, $\mathbf{H}$, and magnetic flux density, $\mathbf{B}$, are related by $\mathbf{B} = \mu_0 \mu_r \mathbf{H}$ where μ_0 and μ_r are the magnetic permeability of free space and relative permeability, respectively. For all of the cases shown in this paper, $\mu_r = 1$. Here, $\mathbf{A}$ is the magnetic vector potential while t is time and $\mathbf{J_e}$ represents the external current density. Numerical solutions in the time domain require an initial condition and are obtained at a series of time steps thereafter. The Comsol AC/DC module uses the temporal or Weyl gauge in which the electrical scalar potential is set to 0.

In the frequency domain, Ampère's law as solved in Comsol reads

$$(i\omega\sigma - \omega^2 \epsilon_0 \epsilon_r)\mathbf{A} + \nabla \times \mathbf{H} = \mathbf{J_e} \tag{3}$$

where ω is the angular frequency, $i = \sqrt{-1}$ and ϵ_0 and ϵ_r are the electrical permittivity of free space and the relative permittivity. For all calculations shown here, we use $\epsilon_r = 1$. Note also that the term describing displacement currents has been retained in equation 3 although it is generally very small at the low frequencies of interest in geophysics. Solutions in the frequency domain are effectively stationary for each frequency but have real and imaginary parts representing harmonic solutions that are in phase and ninety degrees out of phase with some reference.

If a stationary study is used, the form of Ampère's law solved in Comsol becomes

$$\nabla \times \mathbf{H} = \mathbf{J_e}. \tag{4}$$

All solutions were run using Comsol 5.0 on a laptop with a quad core i7 processor running at 2.4 GHz with 24 Gbytes of memory.

In numerical modeling, it is important to have sufficient resolution that there are at least a few elements over the distance on which the fields are changing. The distance over which fields change can be estimate in the frequency domain by the skin depth, $\delta = \sqrt{2\rho/(\omega\mu_0)}$, and in the time domain by the diffusion distance, $\sqrt{\rho t/\mu_0}$, where t is the shortest time scale of interest (e.g., *Telford et al.*, 1991). It is also important to use a simulation domain that is sufficiently large that the outer boundary conditions are not significantly affecting the solution. This means that in the frequency and time domains, the outer boundaries must be at least a few skin depths or a few diffusion distances from the region of interest(where t is now the total time of the simulation).

In all of the simulations shown, the default numerical solver chosen in Comsol was used as well as the default parameter settings. For the MMR simulations, the default solver for the magnetic field is FGMRES (flexible generalized minimal residual) while for the rest of the simulations, it is BiCGStab (stabilized biconjugate gradient). Multigrid with SOR (successive over-relaxation) presmoothers are used as preconditioners for the steady magnetic fields cases

while Multigrid with SOR vector presmoothers are used as preconditioners for the frequency-domain and time-domain simulations. Comsol has built in MUMPS (MUltifrontal Massively Parallel Sparse), PARDISO (Parallel Direct Sparse Solver) and SPOOLES (Sparse Object-Oriented Linear Equation Solver) solvers that can be chosen in lieu of the iterative solver sequence. We experimented with direct solvers for some Very Low Frequency and frequency domain induction simulations. While these direct solvers found good solutions, they typically used 3 to 4 times as much memory and took two to three times as long. Tetrahedral elements were also used in all of the simulations shown. In all cases except for magnetometric resistivity, we did not decompose our solutions into primary and secondary parts.

3. Magnetometric Resistivity

In magnetometric resistivity (MMR), current is injected into the ground at very low frequency between two grounded electrodes. The magnetic field produced by the currents in the ground is measured. The currents are varied sufficiently slowly that induction effects can be ignored. The governing equations consist of those for electrical conduction,

$$\nabla \cdot \sigma \nabla V = I[\delta(\mathbf{r} - \mathbf{r_A}) - \delta(\mathbf{r} - \mathbf{r_B})], \tag{5}$$

and equation 4 where $\mathbf{J_e} = -\sigma \nabla V$.

Equation 5 can be solved using the Electric Currents functionality in Comsol. A spherical domain is used and a plane, drawn using the work plane functionality, is used to divide the upper, air, region from the lower, ground, region. The Electrical Currents solution is chosen to be active only in the lower region since the resistivity of the air is effectively infinite and so its effects can be modeled by specifying a no flux electrical currents boundary condition at the ground surface. The electrodes are modeled as point current sources. In order to achieve more accurate results when using point current sources, it is necessary to greatly refine the grid in the vicinity of the current electrodes. This can

be done in Comsol by selecting a "Free Tetrahedral" mesh and setting the size to work on a point geometrical level and setting a small maximum element size.

The outer boundary condition for the electrical currents in the ground is given by $\mathbf{J} \cdot \hat{\mathbf{n}} = -\sigma V/r$ (*Dey and Morrison*, 1979). Here, $\hat{\mathbf{n}}$ is a unit normal vector while r is the radial distance from the center of the domain. The solution of the magnetic fields is found in both the ground and the air. The domain is made large enough that effects due to the outer boundary do not strongly effect the region of interest. It was found that specifying 0 tangential components of the magnetic field gave superior results to specifying 0 normal component of the magnetic field on the outer boundaries.

While the formulation above worked and solutions were in reasonable agreement with published benchmarks for vertical contacts and vertical dykes (*Edwards and Howell*, 1976), the solutions had a significant degree of resolution-scale noise. It was found that much smoother solutions were obtained by using the formulation of the electrical conduction problem of *Coggon* (1971) where we solve for the variation of the electrical potential, V_s, from that of a constant resistivity background, V_p, in a region with piece-wise constant conductivity. Using this formulation, the point sources do not have to be modeled and the governing equation for V_s within regions of constant conductivity reduces to Laplace's equation. Jump conditions arise at boundaries where conductivity changes discontinuously that take the form

$$(\sigma^+ \nabla V_s^+ - \sigma^- \nabla V_s^-) \cdot \hat{\mathbf{n}} = -\Delta\sigma \nabla V_p|_{\mathbf{r_{bo}}} \cdot \hat{\mathbf{n}}. \tag{6}$$

In equation 6, $\mathbf{r_{bo}}$ represents the position of a boundary where conductivity changes discontinuously while $\Delta\sigma$ represents the jump in conductivity across the boundary. The formulation involving the secondary potential was also used in the finite-element, unstructured grid, 3D resistivity simulations of *Rücker et al.* (2006). A further advantage of the secondary potential formulation is the elimination of the need for a refined grid in the vicinity of the point current sources.

The background potential and its gradients can be calculated analytically using the well-known form for the potential of a point source in an infinite homogeneous half space (e.g., *Telford et al.*, 1991). Equation 6 can be implemented in Comsol using Boundary Currents.

It is customary in MMR analysis to calculate the anomalous magnetic field which is calculated from

$$\mathbf{H^a} = (\mathbf{H_{meas}} - \mathbf{H_{hom}})/H_{yhommax} \tag{7}$$

where $\mathbf{H_{meas}}$ is the measured magnetic field, $\mathbf{H_{hom}}$ is the magnetic field for a homogeneous half space and $H_{yhommax}$ is the horizontal magnetic field for a homogeneous half-space that is midway between the two electrodes.

When solving the current conservation equations in the form of 6, the quantity $(\mathbf{H_{meas}} - \mathbf{H_{hom}})$ can be calculated from equation 4 by setting $\mathbf{J_e} = \sigma\nabla V_s + (\sigma - \sigma_0)\nabla V_p$.

The mesh along the ground surface was refined compared with the rest of the domain. A total of 500000 degrees of freedom were solved for and solutions used roughly 2 GB and took roughly 1 minute.

In figure 1, the results of calculation of H_z^a for a vertical dyke model are compared for three different resistivity contrasts with the results of an analytical model (*Edwards and Howell*, 1976). The dyke is 10 m wide and the current electrodes are positioned 60 m apart along the midline of the dyke. The resistivity of the air is set at 10^8 Ωm. The results can be seen to be in very good agreement. In figure 2, a surface plot of H_y^a is shown along with streamlines of $\mathbf{H^a}$ for the dyke model with resistivity 20 Ωm outside the dyke.

4. The Very Low Frequency Method (VLF) and Magnetotellurics

In "far field methods" the signal source is well approximated as a plane wave. Magnetotellurics and the Very Low Frequency (VLF) method are commonly used far field methods. VLF waves are broadcast for the purpose of communicating with submarines at discrete frequencies near 20 kHz (*McNeil and Labson*,

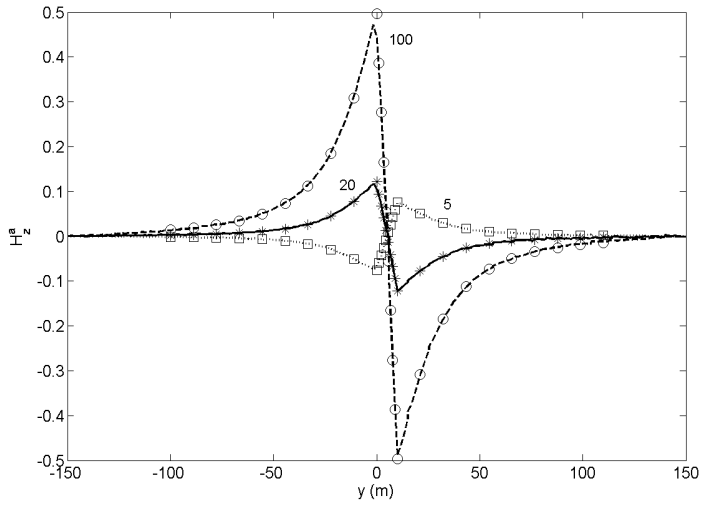

Figure 1: Comparison of the vertical magnetic field MMR anomaly for a vertical dyke with the electrodes along the centre line. The resistivity of the dyke is 10 Ωm while the resistivity of the material outside the dyke, ρ_1, is shown on the figure in Ωm. Dashed, solid and dotted lines show the results of numerical models while symbols show analytical solutions.

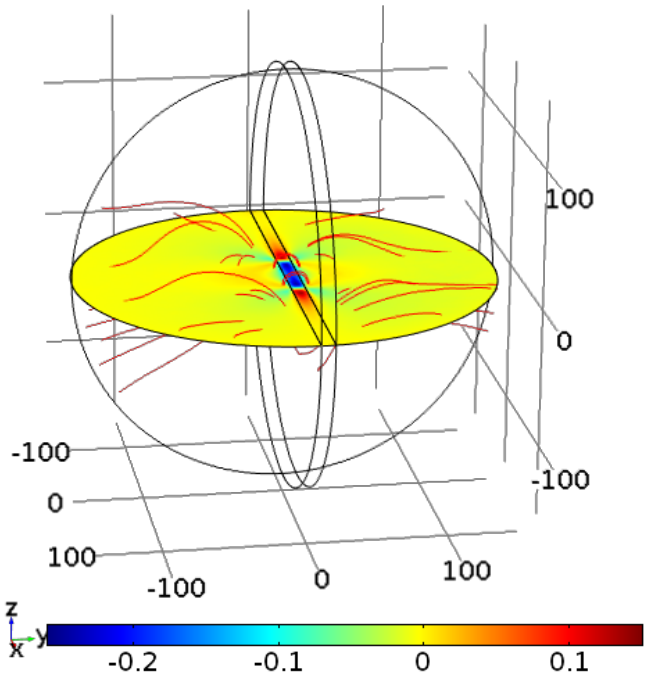

Figure 2: The surface plot shows H_y^a while the streamlines are $\mathbf{H^a}$ for a model of a dyke that is 10 m wide and has resistivity 10 Ω m. The material outside the dyke has resistivity 20 Ωm. The current electrodes are 60 m apart. Blue colors are negative while red are positive.

1991) and so a frequency domain study is chosen. The source for the magnetotelluric method consist of varying magnetic fields in Earth's atmosphere and magnetosphere which are typically decomposed into specific frequencies in the range 10^{-3} Hz to 10^{4} Hz (*Vozoff*, 1991).

A rectangular prism domain is chosen that includes both a region with 0 electrical conductivity in the air ($z < 0$) and a region representing the ground ($z > 0$). The excitation for the model is provided by specifying the analytical solution for the magnetic field over a layered half space on the outer boundaries of the model using the magnetic field boundary condition of Comsol. In using this boundary condition, it is assumed that lateral conductivity variations within the simulation volume, or variations in topography, cause perturbations that die out as one moves towards the boundaries and should therefore be a few electromagnetic skin-depths from the boundary.

If the wave is propagating in the x direction over multi-layer ground then the y component of the analytical expression for the magnetic field is given by (*McNeil and Labson*, 1991)

$$\begin{aligned} H_{0y} &= (a_0 e^{-u_0 z} + b_0 e^{u_0 z}) e^{-i\lambda x} \text{for } \; z < 0 \\ H_{iy} &= (a_i e^{-u_i z} + b_i e^{u_i z}) e^{-i\lambda x} \text{for } \; z > 0. \end{aligned} \tag{8}$$

Here, $i = 1, 2..$ is an index indicating the layer in the ground and $k_i = (\omega^2 \mu_0 \epsilon_0 - i\omega\mu_0\sigma_i)^{1/2}$, $\lambda = k_0 \sin\theta_i$ and $u_i = \lambda^2 - k_i^2$. The quantity θ_i is the angle of incidence with which the wave impinges on the ground surface and is usually close to 90°. While magnetic and electric fields can depend on the angle of incidence, most VLF observables are ratios and most quantities change at the same rate with θ_i and so VLF observables do not change strongly with the angle of incidence. In all of the calculations shown here, $\theta_i = \pi/2 - \pi/40$.

The coefficients a_i and b_i are determined by requiring the continuity of the horizontal components of $\mathbf{H}$ and $\mathbf{E}$ at each horizontal interface where the electrical conductivity changes discontinuously. The electric field can be calculated from the magnetic field using Ampère's Law

$$\mathbf{E} = \frac{\nabla \times \mathbf{H}}{\sigma + i\omega\epsilon_0}. \tag{9}$$

The coefficient of the incoming wave in the air, a_0, is arbitrarily set to 1.

As a first test, models were run at 20 kHz with resistivity variations in layers only. Since analytical solutions for the magnetic field are specified on the boundaries, in these simulations there should be no lateral variations of the magnetic or electric fields within the simulation domain and so the vertical profiles of the magnetic field at the centre of the domain should be exactly the same as the analytical profiles specified on the boundaries. In figure 3, we show the real (solid line) and imaginary (dotted line) parts of the horizontal component of the magnetic field from the horizontal centre of the numerical model as well as those from the analytical solution (circles and asterisks). The region $z < 0$ represents the air which was infinitely resistive, while the region $0 < z < 20$m had resistivity 100 Ωm and the region $z > 20$m had resistivity 10 Ωm. The numerical and analytical models clearly match very well. At the layer interfaces, the slope of H_y can be seen to change discontinuously and the magnetic field can be seen to decay more rapidly in the lower, more conductive, layer.

We next compare the results of our numerical model with the published 2D results of *Baranwal et al.* (2011) who showed calculations with both conductive anomalies and topographic relief. The model geometry as well as the finite element mesh is shown in figure 4. A domain of size 1600 by 1600 by 800 m (vertical) was used.

In order to model the effects of surface topography, an interpolation function was created in Comsol using data points for the topography model used in *Baranwal et al.* (2011) that varied only in the y direction. This interpolation function was then used as the vertical coordinate in a parameterized surface in Comsol that defined the ground surface in the model. Two rectangular prism anomalies were also modeled in the subsurface with resistivities of 20 and 100 Ωm in ground with resistivity 1000 Ωm otherwise. Frequencies of 5, 16 and

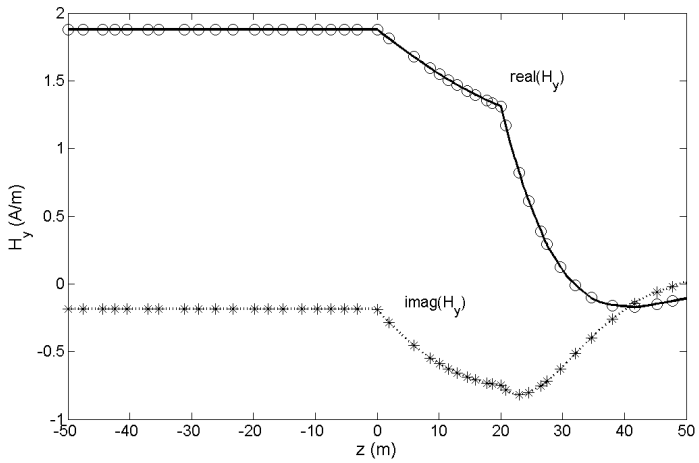

Figure 3: The real (solid line) and imaginary (dotted line) profiles of the horizontal component of the magnetic field for ground with resistivity 100 Ω m above 20 m ($0 < z < 20$m) and 10 Ωm below 20 m at the horizontal center of the model. Circles and asterisks show the analytical solutions for the real and imaginary parts of H_y. The region $z < 0$ is air which is treated as infinitely resistive.

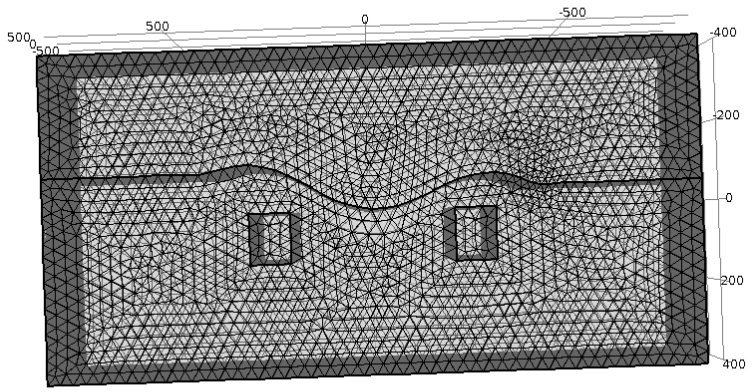

Figure 4: The geometry of the VLF simulation with topography and two resistivity anomalies benchmark with the results of *Baranwal et al.* (2011). The geometry is 3D but there are no changes in the x direction. The tetrahedral elements are shown.

25 kHz were modeled as in *Baranwal et al.* (2011). In figure 5 parts a) and b) our numerical model results for the in phase (I.P.) anomaly (the real part of the vertical component of the magnetic field normalized by the horizontal component of the magnetic field) and ϕ, the phase difference between the x component of the electric field and the y component of the magnetic field at the ground surface. Both of these quantities are commonly used as diagnostics in VLF surveys. As can be seen, our numerical model results are in reasonably good agreement with those of *Baranwal et al.* (2011). The mesh used was roughly 1/3 of the skin depth for the highest frequency in the region with background resistivity. Simulations took roughly 1/2 hour to run and used 17 million degrees of freedom and required 20 GBytes of memory. Note that our simulation was 3D but contained topographic and resistivity variations in 2D only. Our model can easily be used to investigate 3D structure, however.

At the lower frequencies used in magnetotellurics, it becomes more difficult to achieve a converged solution using Magnetic Fields solvers in Comsol. It was found that for a single layer Earth model, the domain size needed to be at least two skin depths in size for a model run at 100 Hz while at 0.01 Hz, a domain of size 20 skin depths was needed in order to achieve convergence. At low frequencies, the horizontal component of the electric field in the air becomes especially numerically noisy. Comsol Multiphysics has a magnetotellurics model as one of its sample models which we will hereafter refer to as model CMM. In CMM, the air is not modelled and one horizontal component of the magnetic field is specified as constant at the ground surface. When there is a horizontal variation in electrical resistivity in the direction of the main horizontal magnetic field, there will be horizontal variations in the magnitude of the horizontal magnetic field (*MacNeil and Labson*, 1991) and so there will be some errors in the CMM model.

In magnetotellurics, it is common to calculate the apparent resistivity for waves propagating in the x and y directions from

$$\rho_{xy} = (\frac{E_x}{H_y})^2/(\omega\mu_0), \tag{10}$$

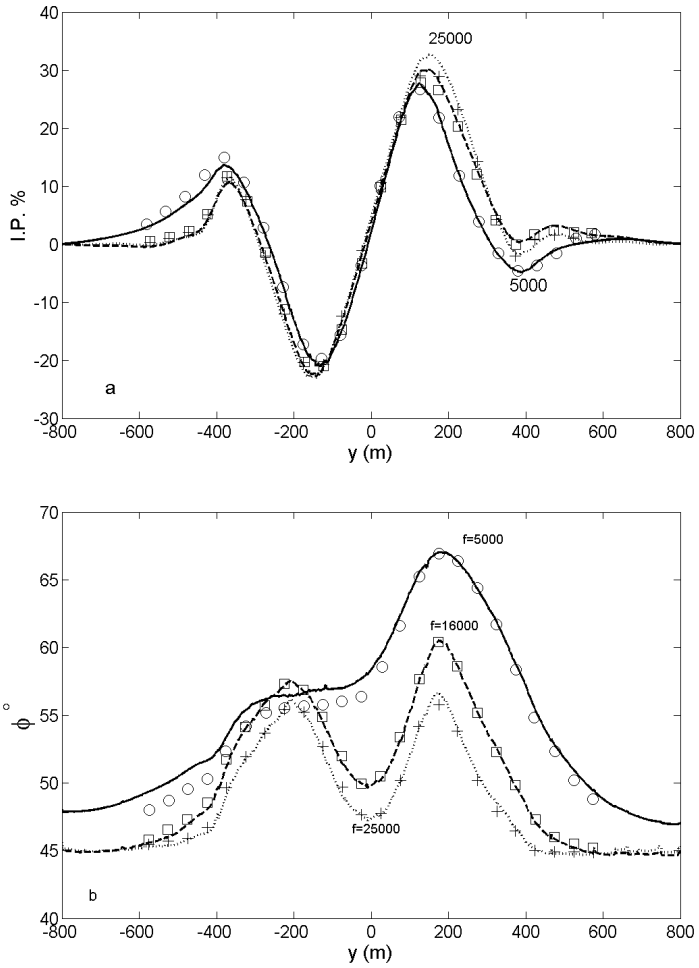

Figure 5: Comparison of our results (lines) with those of *Baranwal et al.* (2011) for VLF over topography and anomalous conductors. a) The in-phase anomaly b) the phase difference between the horizontal electrical field and the horizontal magnetic field.

and

$$\rho_{yx} = (\frac{E_y}{H_x})^2/(\omega\mu_0), \tag{11}$$

respectively. Models were run using both the formulation presented here and CMM using the geometry of model 3D-1A from the COMMENI project (*Zhdanov et al.*, 1997) which consists of a rectangular prism of resistivity 0.5 Ωm and side lengths 1 km (x direction), 2 km (y direction) and 2 km (z direction) in a medium with resistivity 100 Ω m. Simulations were run with wave propagation along both the x and y axis directions.

In figure 6 we present the average of the results presented in *Zhdanov et al.* (1997) (symbols), as well as results calculated using CMM (solid and dash-dot lines) and the model presented here (dotted and dashed lines). The values of ρ_{xy} (solid and dashed lines) and ρ_{yx} (dash and dash-dot lines) are plotted along the x axis for frequencies of 10 Hz (thin lines) and 0.1 Hz (thick lines). While both sets of simulations are numerically noisy, the formulation presented here shows somewhat better agreement with the results of *Zhdanov et al.* (1997) particularly at the lower frequency. The finite-element mesh was refined at the ground interface and in the conducting anomaly. Simulations had 550000 degrees of freedom, used 2.57 GBytes and took roughly 1 minute to run. For the low frequency simulations, the relative tolerance for convergence had to be reduced to 1 in order to achieve a solution. The outer dimensions of the model were size 20 km by 20km by 40km (high). The COMMENI3D1A problem has also been investigated by *Ren et al.* (2013) and *Grayver and Bürg* (2014) and their results were in close agreement with those of *Zhdanov et al.* (1997).

5. Frequency Domain Electromagnetics

Frequency domain electromagnetic techniques employ an AC electrical current in a wire coil as a transmitter. The alternating magnetic field of the transmitter induces alternating electrical currents in the ground that are then detected using a second induction coil. The depth of investigation varies with the

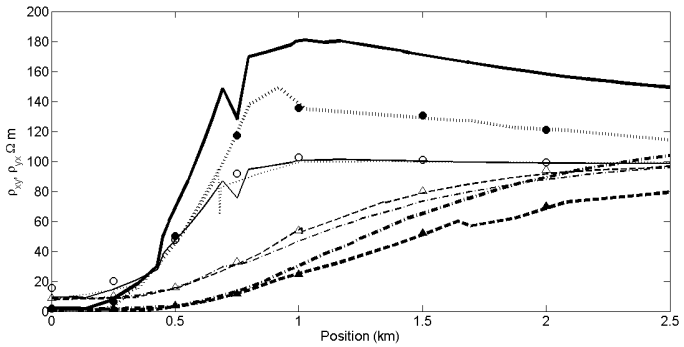

Figure 6: Comparison between results using the model presented here, model CMM and the results presented in *Zhdanov et al.* (1997) for model 3D1A of *Zhdanov et al.* (1997). Circles and triangles are results of *Zhdanov et al.* (1997) for ρ_{xy} and ρ_{yx} along the x axix. Filled and open symbols are for simulations run at 0.1 and 10 Hz. Results for ρ_{xy} from simulations run with the model presented here and CMM are represented by dotted and solid lines, respectively. Results for ρ_{yx} from simulations run with the model presented here and CMM are represented by dashed and dash-dot lines, respectively. Thick and thin lines represent simulations run using 0.1 Hz and 10 Hz frequency, respectively.

frequency of the current used in the transmitter and the transmitter-receiver distance (*Telford et al.*, 1991).

As a first test, we approximate the transmitter as a vertical magnetic dipole situated at the surface of a homogeneous infinite half-space.. We compare the numerical results with a solution for a vertical dipole at the origin above an infinite half space of constant conductivity (*Ward and Hohmann*, 1988),

$$H_z = \frac{m}{2\pi k^2 r_c^5}[9 - (9 + 9ikr_c - 4k^2r_c^2 - ik^3r_c^3)e^{-ikr_c}]. \tag{12}$$

Equation 12 is valid at $z = 0$ while r_c is the radial distance from the dipole and k has the same definition as in the VLF section.

A spherical domain of radius 1000 m was used which was again divided by a circle into a lower half representing ground with resistivity 100 Ω, and an upper half with resistivity 10^8 Ωm representing air. The dipole was modeled using the point dipole capability of Comsol and the outer boundaries were set to

have 0 tangential components of the magnetic field using the "Magnetic Fields" boundary condition in Comsol.

The model mesh was refined in the neighbourhood of the dipole and at the ground surface. Frequencies of 100, 1000, 10^4 and 10^5 Hz were used which correspond to electromagnetic skin depths of 503, 159, 50, and 15.9 m.

In figure 7, a vertical slice of the real part of the component of the electrical current density that is perpendicular to the slice is shown as well as streamlines and arrows showing the real parts of the magnetic field and the electrical current density when the frequency is 100 Hz.

In frequency-domain electromagnetics, it is customary to plot the secondary fields, which correspond to the measured fields with the fields produced by the transmitter in the absence of any conductors subtracted. When normalized, these quantities for the vertical component of the magnetic field are

$$IP = \frac{real(H_z) - H_z^{dip}}{H_z^{dip}} \tag{13}$$

and

$$Quad = \frac{imag(H_z)}{H_z^{dip}} \tag{14}$$

where H_z^{dip} is the vertical magnetic field of a dipole in the absence of conductors.

In figure 8, we show profiles of normalized fields, IP and Quad, from our model (lines) and using the analytical solution from equation 12 (symbols). As can be seen in the IP plot in particular, there is a significant degree of numerical noise near the dipole source. The quality of the solution near the dipole source could be improved by increasing the resolution in this region but at a significant cost in computation time. It can also be seen for the low frequency simulations that the numerical and analytical solutions differ when they are within one skin depth of the outer boundary. Some simulations were undertaken with Comsol's "infinite elements", volumes on the exterior where the solution is stretched to infinity, but only the lower frequency solution was improved near the outer boundaries and the processing time was longer.

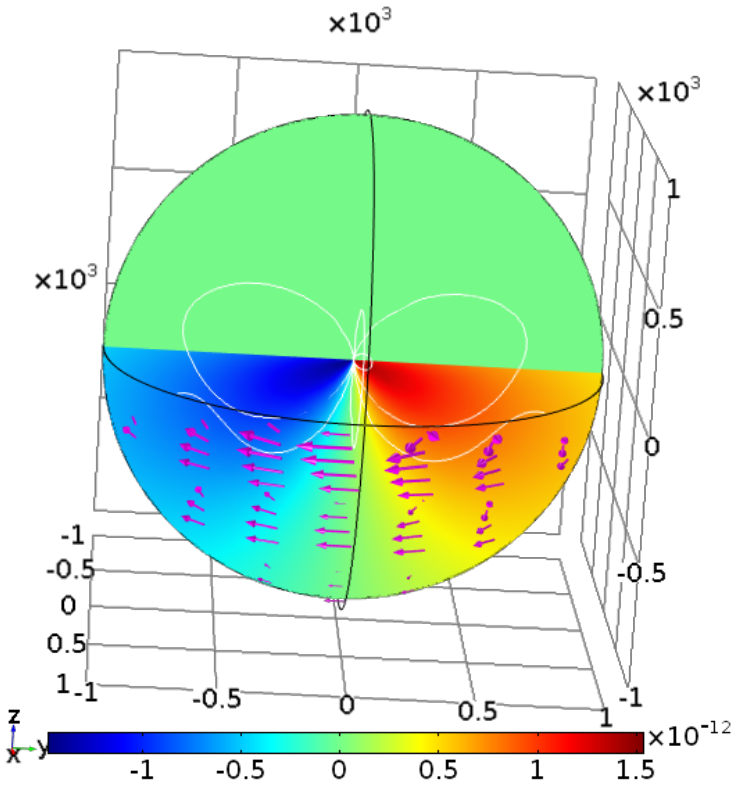

Figure 7: A vertical slice plot of the real part of the electrical current density that is perpendicular to the slice as well as streamlines of the magnetic field and arrows showing the electrical current density in the ground for frequency 100 Hz. Red colors are positive while blue are negative.

Generally the numerical and analytical results are in very good agreement. The solution for all four frequencies involved solving for three million degrees of freedom and took 16 minutes.

Ansari and Farquharson (2014) showed finite element solutions for the secondary magnetic field above a cube of conductivity 63000 S/m and side length 14 cm immersed so that its top surface was 2 cm below the surface of brine with conductivity 7.3 S/m. The simulations were set up to model a physical scale model and their numerical results were seen to be in good agreement with the physical scale model as well as with results of integral-equation methods (*Farquharson et al.*, 2005) and finite-volume simulations (*Jahandari and Farquharson*, 2014). The transmitter was a vertical dipole that was positioned in air 2 cm above the brine while the receiver measured the vertical component of the magnetic field at a distance of 20 cm.

It can be difficult to mesh good conductors adequately since the skin depth is very small for these objects. *Ansari and Farquharson* (2014) used a very high density of elements within the conducting cube. In the frequency domain, Comsol has the capability to represent thin conductors using effective boundary conditions known as "Transition Boundary Conditions" on planes. Larger conductors can be represented using "Impedance Boundary Conditions" on the boundaries of a volume. The inside of the volume is not included in the calculation. In order to compare with the simulations of *Ansari and Farquharson* (2014), the conductive cube was represented by applying 6 impedance boundary conditions on the boundaries of the cube. The transmitters were represented using Comsol's "Point Dipole" capability and calculations were carried out for each transmitter position by specifying the dipole moment for each transmitter to be non-zero for only one calculation of a parameter study. The simulation domain was set to be of size 10 skin-depths for the brine conductivity while the mesh was also made finer in the vicinity of the dipoles (maximum element size 0.01m), on the brine-air interface (mesh size set to "extremely fine") and on the edges of the block (maximum element size 0.01m). The resistivity of the air was set to be 10^6 times that of the brine.

In figure 8 the results of our simulation at 100 kHz is compared with the results of *Ansari and Farquharson* (2014). The agreement between the two sets of simulations is very good. Similar agreement was found for frequencies 10 kHz, 200 kHz and 400 kHz. At 200 kHz and below, we had to increase the relative tolerance of the solver to 0.05 from its default value of 0.001 in order to achieve convergence. The solutions were still in good agreement with those of *Ansari and Farquharson* (2014). At frequency 400 kHz, solutions consisted of 640000 degrees of freedom and required 3Gbyts of memory. Solution for 26 dipole positions took 26 minutes. *Ansari and Farquharson* (2014) also presented results at 1 kHz. We were unable to get our solution to converge at this frequency without decreasing the tolerance to the point that the solution no longer matched the benchmark.

We also attempted to find solutions without using the impedance boundary conditions by resolving a skin depth within the conductive block. A solution was obtained for frequency 400 kHZ that was in reasonable agreement with the benchmarks. The solution required roughly three times as many degrees of freedom and took roughly three times as long to compute, indicating the significant advantage of using the impedance boundary conditions.

6. Time Domain Electromagnetics

In time domain electromagnetics, electrical currents are induced in ground by a non-harmonic current variation in a transmitter. In many cases, electrical currents are induced in the ground by the changing magnetic field caused by the abrupt shut-off of transmitter currents. The decay of the ground induction currents is then measured by another induction coil at the ground surface.

In order to benchmark the model, the solution for the transient field caused by the instantaneous shut-off of a vertical dipole at the surface of an homogeneous half space is compared with the analytical solution of *Nabighian and Macnae* (1989). A spherical domain of radius 600 m was used. The initial condition for the magnetic vector potential was that of a steady-state vertical dipole

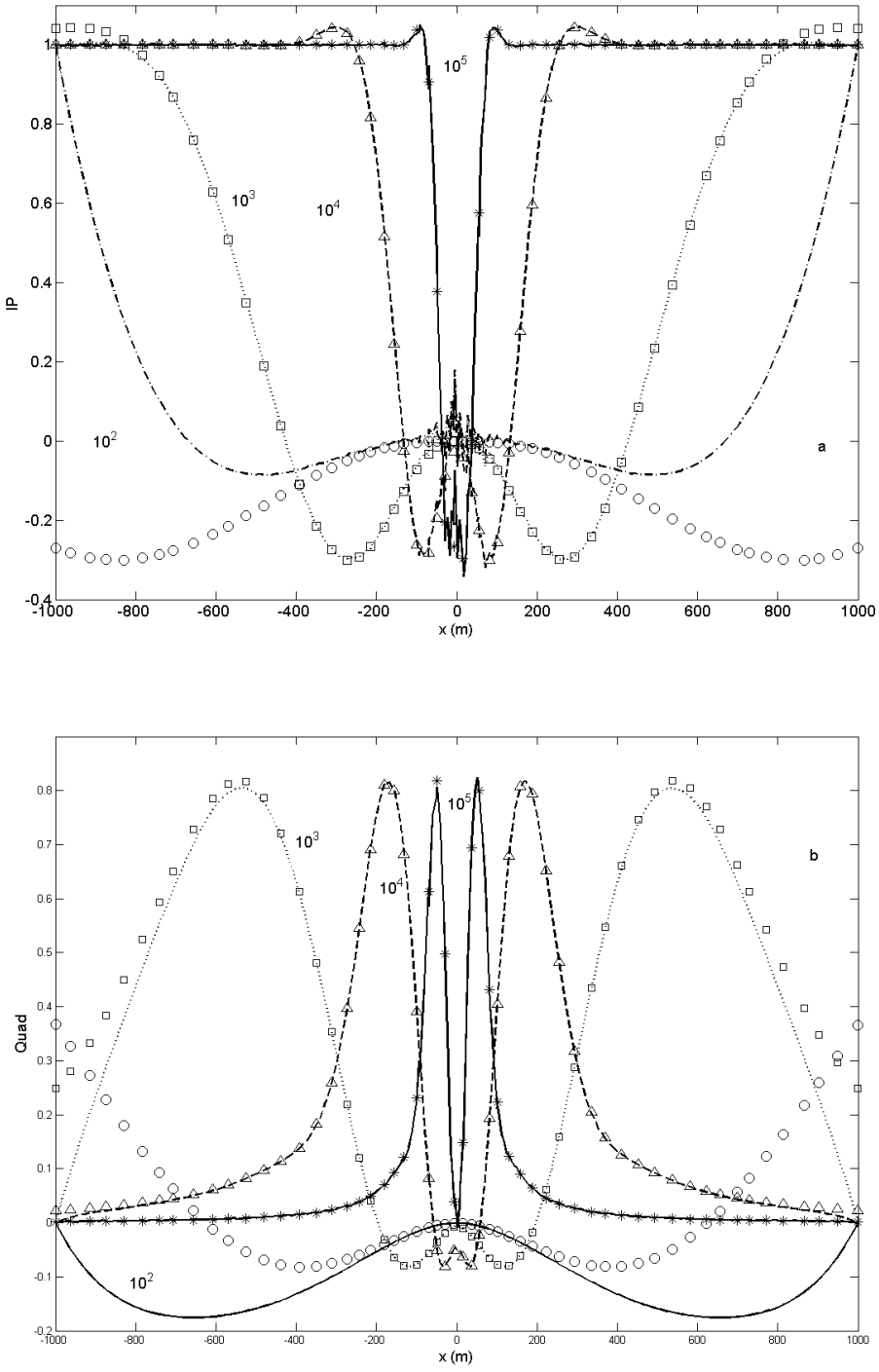

Figure 8: Profiles of a) IP and b) Quad profiles on the ground surface in the x direction at $y = 20$ m from the dipole source, from the numerical model (lines), and from the analytical solution (symbols).

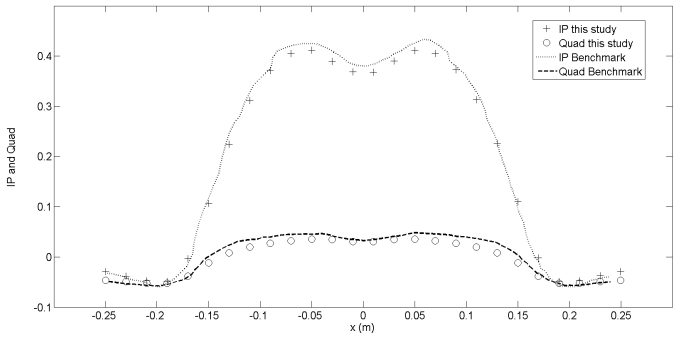

Figure 9: Profile across a conductive target in a conductive medium at frequency 100 kHz. The transmitter and receiver are vertical coplanar loops 20cm apart. The conductor is a cube of side length 14cm and conductivity 63000 S/m. The conductivity of the background is 7.3 S/m. Symbols are the results of a calculation in this study while lines are digitized from the results of *Ansari and Farquharson* (2014).

situated at the origin. The boundary condition specifies 0 tangential components of the magnetic field. Once the integration began, there was no excitation specified and the model computed the transient decay of the field over a uniform half space with resistivity 10 Ωm. In figure 11, the time evolution of the field calculated on the ground surface at points 20, 40, 60 and 80 m away from the dipole (solid lines) is compared with the analytical solution (dotted lines). At early times, the current circulating in the ground is close to the initial dipole. When the current ring has diffused beyond the measuring point, the orientation of the magnetic field changes sign and this causes the cusp in the plot since the absolute value of H_z is taken. The domain size was chosen to be larger than the diffusion distance for the integration time so that the long time decays of the analytical and numerical solutions are very similar. It can also be seen that there is discrepancy between the numerical model and the analytical solution at early times, particularly for the point 20 m from the origin. This is likely due to inadequate resolution of the early decay of the initial dipole field that becomes smoother as the field diffuses outward. In part b) of figure 11 the time

rate of change of the vertical component of the magnetic field is shown and it is also compared with the analytical solution.

The solution took 37 minutes to run on our machine and required 498668 degrees of freedom. In order to get adequate time resolution, we forced Comsol's solver to calculate 100 solutions per decade of time between 10^{-6} and 10^{-2} s by selecting "strict" time stepping. It can be seen that there is slightly more error at early times for dH_z/dt but the numerical solution for this field is not affected by the outer boundaries until later. Runs were also carried out with the magnetic insulation boundary condition (requiring that the tangential components of $\mathbf{A}$ were 0) but these gave greater errors than specifying the tangential components of the magnetic field to be 0.

In the time domain, Comsol does not have the functionality to include isolated conductors through boundary conditions so anomalies must be made of finite size. It is therefore necessary to refine the mesh within the conductive anomaly so that there were at least a few elements per diffusion distance.

In figure 12 we show $\frac{dH_z}{dt}$ from simulations initiated with the field of a steady dipole over ground with a) a conductive dyke ($\rho_c = 1$ Ωm and b) a resistive dyke $\rho_c = 100$ Ω m. The solution can be seen to differ from circular symmetry because of the effect of the dyke. With the conductive anomaly, the field can be seen to be decaying more slowly (less blue colors) in the anomaly than the backgroud case while the opposite is true for the resistive anomaly.

Time domain simulations were also carried out using currents within the simulation domain as excitations. These were introduced using the "Edge Currents" capability in Comsol around current loops.

A time-domain simulation with infinite elements was also run. It was found that the simulation became extremely slow at long times as the solution near the boundary differed significantly from 0. It is probably best to just use no tangential magnetic field boundary conditions and make the domain size significantly larger than one diffusion distance.

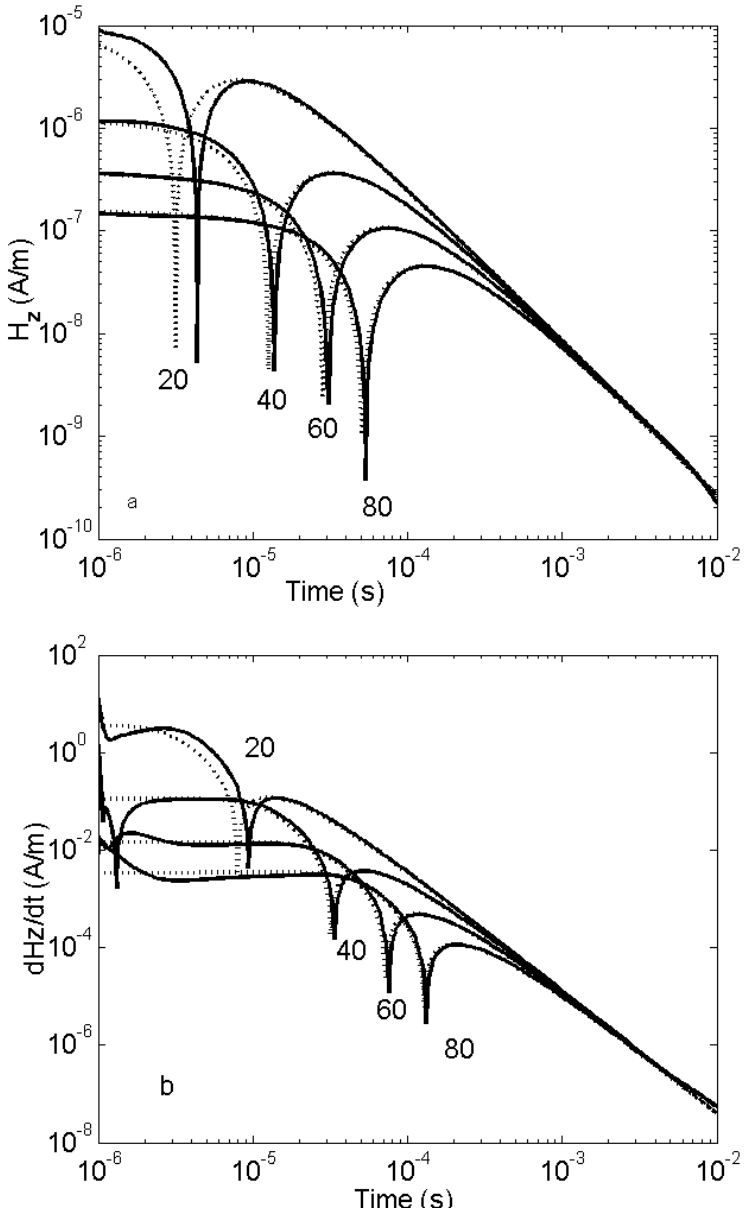

Figure 10: a) Decay of the vertical component of the magnetic field calculated from the numerical model (solid lines) and the analytical solution (dotted lines) for the instantaneous shut-off of a steady dipole magnetic field at the ground surface for an infinite half-space of resistivity 1 Ωm. b) $|dH_z/dt|$. Distances in m of the points from the dipole are inidicated on the figure.

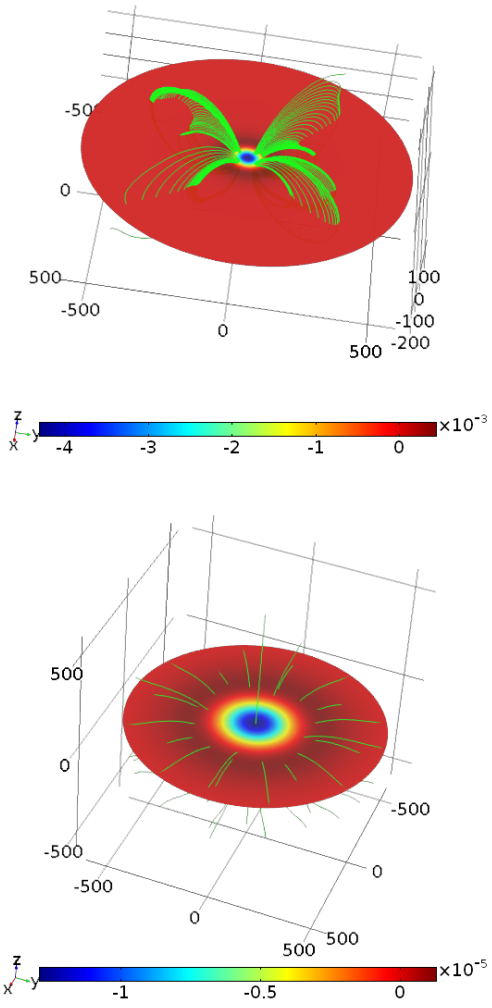

Figure 11: a) Slice plot of $\frac{dH_z}{dt}$ on the ground surface and streamlines of the magnetic field at times a) 1×10^{-4}s, b) 5×10^{-3}s from a simulation with homogeneous ground with resistivity 10 Ωm.

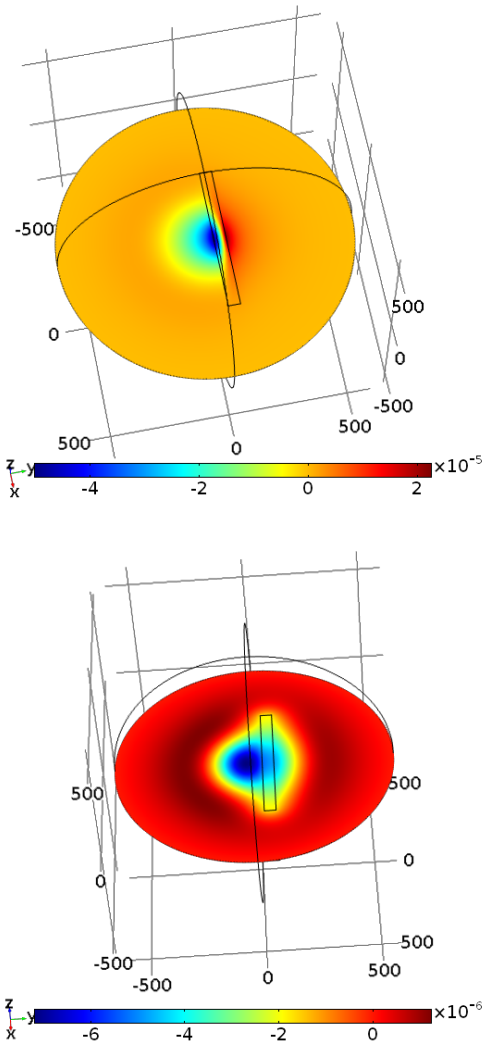

Figure 12: a) Slice plot of $\frac{dH_z}{dt}$ on the ground surface y at time 1×10^{-3}s for a simulation with a) a conductive anomaly b) a resistive anomaly.

7. Conclusions

We have shown examples of forward calculations of various electromagnetic geophysical methods using Comsol Multiphysics and in all cases, the calculations are in good agreement with benchmarks and previously published results. All of the simulations ran in less than one hour on a commodity laptop computer with 24 Gbytes of RAM, a configuration that is easily accessible to most users nowadays. While this time may be too long for use in an inversion scheme, these models take much less human time to set up and so new configurations can be quickly and easily prototyped. These simulations can also be easily set up for use in classes.

An advantage in using Comsol is that it takes a relatively short period of time to create the models. Most published research in geophysical electromagnetic modeling involves dedicated research codes. There exists a dedicated commercial software package called Maxwell for geophysical electromagnetic modeling that runs very quickly and has built-in configurations of common frequency and time-domain electromagnetic equipment. However, Maxwell only accounts for the effects of isolated conductors and does not take into account that the ground has a finite conductivity. It is also not easily configured to unconventional set-ups.

We expect that geophysical modeling of electromagnetic techniques using Comsol will be very useful, particularly for researching new configurations and for pedagogical purposes.

8. References

Ansari, S., and C.G. Farquharson, 2014,3D finite-element forward modeling of electromagnetic data using vector and scalar potentials and unstructured grids, *Geophysics*, 79, E149-E165, doi: 10.1190/geo2013-0172.1

Avdeev, D.B., 2005, Three-dimensional electromagnetic modelling and inversion from theory to application, *Surv. Geophys.*, **26**, 767-799.

Avdeev, D., and S. Knizhnik, 2009, 3D integral equation modeling with a linear

459 dependence on dimensions, *Geophysics*, **74**, F89F94, doi: 10.1190/1.3190132.
460 Borner, R.U., 2010, Numerical Modelling in Geo-Electromagnetics: Advances
461 and Challenges, *Surv. Geophys.*, **2**, 225-245.
462 Butler, S.L. and G. Sinha, 2012, Forward modeling of applied geophysics meth-
463 ods using Comsol and comparison with analytical and laboratory analog models,
464 Computers and Geosciences, **42**, 168-176.
465 Comsol Multiphysics User's Guide, 2014, Comsol Multiphysics User's Guide,
466 2014, Version 5.0, Comsol AB, Stockholm, Sweden.
467 Coggon, J.H., 1971, Electromagnetic and Electrical Modeling by the Finite El-
468 ement Method, *Geophysics*, **36**, 132-155.
469 Dey, A., and Morrison, H.F., 1979, Resistivity modeling for arbitrarily shaped
470 three-dimensional structures, *Geophysics*, **44**, 753-780.
471 Edwards, R.N., and E.C. Howell, 1976, A field test of the magnetometric resis-
472 tivity (MMR) method, *Geophysics*, *41*, 1170-1183.
473 Farquharson, C.G., K. Duckworth and D.W. Oldenburg, 2006, Comparison of
474 integral equation and physical scale modeling of the electromagnetic responses
475 of models with large conductivity contrasts: Geophysics, 71, no. 4, G169G177,
476 doi: 10.1190/1.2210847.GPYSA70016-8033.
477 Grayver, A. and Bürg, M., 2014, Robust and scalable 3-D geo-electromagnetic
478 modelling approach using the finite element method, *Geophys. J. Int.*, 198,
479 110-125, DOI: 10.1093/gji/ggu119.
480 Jahandari, H., and C.G. Farquharson, 2014, A finite-volume solution to the geo-
481 physical electromagnetic forward problem using unstructured grids, **79**, E287-
482 E302, DOI: 10.1190/GEO2013-0312.1.
483 McNeill, J. D., and Labson, V. F., 1991, Geological Mapping Using VLF Ra-
484 dio Fields Electromagnetic Methods in Nabighian, M.N., Ed., Electromagnetic
485 methods in applied geophysics, 2, Soc. Expl. Geophys., 521-587.
486 Nabighian, M.N. and Macnae, J.C., 1989, Time-domain electromagnetic prospect-
487 ing methods, in Nabighian, M.N., Ed., Electromagnetic methods in applied geo-
488 physics, 2, Soc. Expl. Geophys.
489 Ren, Z., Kalscheuer, T., Greenhalgh, S. and Maurer, H., 2013, A goal-oriented

adaptive finite-element approach for plane wave 3-D electromagnetic modelling, *Geophys. J. Int.*, 194, 700-718, doi: 10.1093/gji/ggt154.

Reynolds, J., 2011, An introduction to applied and environmental geophysics, Wiley-Blackwell.

Rücker, C., T. Günther, and K. Spitzer, 2006, Three-dimensional modelling and inversion of dc resistivity data incorporating topography - I. Modelling, *Geophys. J. Int.*, **166**, 495-505, doi: 10.1111/j.1365-246X.2006.03010.x.

Smith, R., 2014, Electromagetic Induction Methods in Mining Geophysics from 2008-2012, *Surv. Geophys.*, **35**, 123-156.

Strack, K.M., 2014, Future Directions of Electromagnetic Methods for Hydrocarbon Applications, *Surv. Geophys.*, **35**, 157-177.

Telford W.M., L.P. Geldardt, and R.E. Sheriff, 1990, Applied Geophysics 2nd Edition, Cambridge University Press.

Vozoff, K., The magnetotelluric method,in Nabighian, M.N., Ed., Electromagnetic methods in applied geophysics, 2, Soc. Expl. Geophys., 641-711.

Wang, T., and G. W. Hohmann, 1993, A finite-difference time-domain solution for three-dimensional electromagnetic modeling, *Geophysics*, **58**, 797809, doi: 10.1190/1.1443465.

Ward, S. H., and G. W. Hohmann, 1988, Electromagnetic theory for geophysical applications, in Nabighian, M. N., ed.,*Electromagnetic methods in applied geophysics: Volume 1, Theory: SEG*, 130311.

West, G., and J. C. Macnae, 1991, Physics of the electromagnetic induction exploration method, in Nabighian, M. N., ed., *Electromagnetic methods in applied geophysics: Volume 2, Application: SEG*, 545.

Zhdanov, M.S., I.M. Varentsov, J.T. Weaver, N.G. Golubev, and V.A. Krylov, 1997, Methods for modelling electromagnetic fields Results from COMMENI–the international project on the comparison of modelling methods for electromagnetic induction, *J. of Appl. Geophys.*, 133-271.

9. ACKNOWLEDGMENTS

We would like to acknowledge the financial support of the Natural Sciences and Engineering Research Council of Canada. We would also like to thank James Merriam and Han Yu for their input and for the very useful reviews of two anonymous reviewers.